Analysis of barrier inhomogeneities in Ti/p–type strained Si0.95Ge0.05 Schottky diodes using reverse current-voltage characteristics

Mohammed Mamor, Khalid Bouziane, Hind Chakir, Pierre Ruterana

▶ **To cite this version:**

Mohammed Mamor, Khalid Bouziane, Hind Chakir, Pierre Ruterana. Analysis of barrier inhomogeneities in Ti/p–type strained Si0.95Ge0.05 Schottky diodes using reverse current-voltage characteristics. Materials Science in Semiconductor Processing, 2024, 176, pp.108314. 10.1016/j.mssp.2024.108314 . hal-04622015

HAL Id: hal-04622015

https://normandie-univ.hal.science/hal-04622015

Submitted on 24 Jun 2024

HAL is a multi-disciplinary open access archive for the deposit and dissemination of scientific research documents, whether they are published or not. The documents may come from teaching and research institutions in France or abroad, or from public or private research centers.

L'archive ouverte pluridisciplinaire **HAL**, est destinée au dépôt et à la diffusion de documents scientifiques de niveau recherche, publiés ou non, émanant des établissements d'enseignement et de recherche français ou étrangers, des laboratoires publics ou privés.

Distributed under a Creative Commons Attribution 4.0 International License

Analysis of barrier inhomogeneities in Ti/*p*–type strained $Si_{0.95}Ge_{0.05}$ Schottky diodes using reverse current-voltage characteristics

Mohammed Mamor[a,c], Khalid Bouziane[b], Hind Chakir[a,b] and Pierre Ruterana[c]

[a]Laboratoire Physique Fondamentale et Appliquée–Safi (LPFA-Safi), Faculté Poly-Disciplinaire, B. P. 4162 Safi, Université Cadi Ayyad, Marrakech, Morocco.
[b]LERMA, Collège Ingénierie et Architecture, Université Internationale de Rabat, Parc Technopoles Rabat-Shore, 11100 Sala El Jadida, Morocco
[c]CIMAP, UMR 6252, CNRS, ENSICAEN, Université de Caen-Normandie, CEA, 6 Boulevard du Maréchal Juin, 1400 Caen, France.

ABSTRACT

Extracting electrical parameters such as barrier height inhomogeneities (*BH*i) from the forward bias can be very challenging in metal/semiconductor (M/Sc) contacts characterized by low barrier height and high series resistance. In this work we demonstrate that the reverse bias characteristics can be used as an efficient alternative method to investigate the inhomogeneity of low barrier height in M/Sc contacts. In particular, the *BH*i in Ti/*p*-strained $Si_{0.95}Ge_{0.05}$ Schottky barrier diodes (SBD) has been investigated using reverse current–voltage-temperature (I_R-V_R-T) characteristics over the temperature range of 100-300 K. The temperature dependence of the measured barrier heights (Φ_{RBp}) using reverse-bias is successfully explained in terms of a thermionic emission (*TE*) current transport associated with Gaussian distribution of the barrier height due *BH*i. The mean homogeneous barrier height ($\overline{\Phi}_{RBp}$) and its corresponding standard deviation (σ_{Rs}) were determined for different reverse voltages. A decrease in $\overline{\Phi}_{RBp}$and an increase in σ_{Rs} with increasing reverse bias are observed, indicating a large barrier height distribution upon high applied reverse bias. The deduced average zero-field barrier height ($\Phi_{FBp} \approx 0.59$ eV) from I_R-V_R agrees well with the corresponding value determined from the forward characteristics. Moreover, the reverse bias extracted values for Richardson constant A^* based on *BH*i model, are found in fair agreement with the reported theoretical value of 32 A.cm^{-2} K^{-2} for our *p*-type strained $Si_{0.95}Ge_{0.05}$ alloy. Finally, the results obtained on Pd/*n*-type $Si_{0.90}Ge_{0.10}$ structure shown in this work fully support the utilization of such reverse bias method.

*) **Electronic mail: mohammedmamor@yahoo.com; m.mamor@uca.ac.ma**

I. INTRODUCTION

Metal/semiconductor (M/Sc) rectifier contacts namely Schottky barrier diode (SBD) have been for many years a subject of intense research because of their technological interest in electronic and optoelectronic integrated circuits [1-4]. Gaining a better understanding of the behavior of such M/Sc interface is of fundamental and technological importance for developing semiconductor-based devices. The electrical properties of M/Sc contacts on different semiconductors materials are characterized by their Schottky barrier heights (SBH). Numerous works have been devoted to the extraction of the Schottky parameters characterizing M/Sc contacts such as the Schottky barrier height (Φ_B) and the ideality factor (n) [5]. These two latter parameters are usually determined either from forward current-voltage (I_F-V_F) or capacitance-voltage (C-V) measurements [6-15]. By contrast to I_F-V_F characteristics of SBD at room temperature, the temperature dependence of the I_F-V_F characteristics provides better information about the current conduction modes across the M/Sc interface and on the corresponding potential imperfections related to the technological steps during the manufacturing process of devices fabrication. It is worth mentioning that the analysis of the temperature dependent I_F-V_F characteristics of the SBD based on thermionic emission (*TE*) theory reveals usually an abnormal decrease in Φ_B and an increase in n *w*ith the decrease in temperature [12-21]. Attempts have been made to determine the laws which provide the temperature dependence of the two above mentioned parameters. For instance, Werner and Güttler [16] proposed a theory the so-called the inhomogeneous model. Such model explains the fluctuation of the potential barrier associated with a Gaussian distribution characterized by a mean value, ($\overline{\Phi}_B$) and a standard deviation of distribution, (σ_s) of the Schottky barrier. Several reports have interpreted their ballistic electron emission microscopy (BEEM) [22-26] data by using the Werner and Güttler model. More precisely, they demonstrated the presence of the barrier height inhomogeneities (*BHi*) at M/Sc contacts on the basis of the existence of a Gaussian distribution of the barrier heights. It should be stressed out that the forward characteristics ln (I_F) vs. V_F is highly nonlinear due to high series resistance and/or the low

Schottky barrier height either on *p*-type or *n*-type semiconductor, making it difficult to extract the SBH Φ_{Bp}. In fact, the value of Φ_{Bp} might be determined straight forward from the reverse current-voltage (I_R-V_R) characteristics by the measurements of the reverse saturation current at a given applied reverse voltage V_R, and by considering the *TE*, as the mode governing the reverse current transport. The value of Φ_{Bp} is an effective barrier height which depends on the reverse voltage through the image force lowering ($\Delta\Phi_{im}$). It differs also from the zero bias barrier height as deduced from I_F-V_F characteristics under the application of low electric field. Indeed, the reverse current in Schottky contact corresponds to the majority carriers from the metal side towards the semiconductor through the Schottky barrier height. By contrast, to PN junctions where the reverse bias corresponds to the minority carrier current.

Although numerous studies have been performed to investigate the *BH*i on different M/Sc contacts using I_F-V_F characteristics, limited studies of I_R-V_R characteristics are available [27-32]. To our knowledge, the investigation of *BH*i in M/Sc Schottky diodes using temperature dependent reverse electrical characteristics has not been reported in the literature, yet. Therewith I_R-V_R characteristics may be used to investigate the *BH*i and to overcome the drawback related to the usual non-linearity of ln (I_F) versus V_F. This non-linearity is associated with a high series resistance and/or low Schottky barrier height.

In this work, Ti/*p*-strained $Si_{0.95}Ge_{0.05}$ is used as a test structure to investigate the *BH*i using reverse bias in the temperature range of 100–300 K. The junction of this structure has lower Schottky barrier height than the corresponding counterpart on *n*-type $Si_{0.95}Ge_{0.05}$ or *n*-type silicon.

We demonstrate in this work that the reverse method can be successfully used to extract electrical parameters of Ti/*p*-strained $Si_{0.95}Ge_{0.05}$. We show also that the utilization of the reverse bias method is corroborated by the results obtained on Pd/*n*-type $Si_{0.90}Ge_{0.10}$ Schottky barrier diode.

The choice of the Ti/ *p*-strained $Si_{0.95}Ge_{0.05}$ structure is motivated by three main reasons for the purpose of this work: *(i)* the barrier height of the Ti/*p*-strained $Si_{0.95}Ge_{0.05}$ contact is low; since the *p*-type strained $Si_{0.95}Ge_{0.05}$ epilayer has a low band gap with respect to either the relaxed $Si_{0.95}Ge_{0.05}$

epilayer or Si epilayer , *(ii)* low Ge concentration (5%) to avoid relaxed film induced dislocations; which will deteriorate the electrical properties of the Schottky contacts, *(iii)* the choice of Ti characterized by a low work function (Φ_{Ti} = 4.3 eV) [33] in order to obtain a good rectifier Schottky contacts on *p*-type materials. From application point of view, Schottky junctions of Ti on *p*-type strained $Si_{0.95}Ge_{0.05}$ epilayers are of technological interest for infrared detector applications. Indeed, to extend the cutoff wavelength for the infrared detection, a lower barrier height is required in order to detect infrared radiation in the long wavelength region.

II. EXPERIMENTAL DETAILS

The sample used for the SBD fabrication is a 383 nm thick epitaxial strained *p*-type $Si_{0.95}Ge_{0.05}$ layer, doped to about 8×10^{16} boron/cm^3. It was grown by rapid thermal chemical vapor deposition (RTCVD) on a lightly doped (4-6$\times10^{16}$ cm^{-3}) Si buffer layer, which in its turn was grown on an p^+-type thick Si substrate. After chemical cleaning, circular Ti Schottky contacts of 0.77 mm diameter and 100 nm thick were deposited on the strained *p*-type $Si_{0.95}Ge_{0.05}$ epilayer by electron beam evaporation. The ohmic contacts were formed on the p^+-Si substrate using an eutectic In-Ga alloy. A scanning electron microscope (SEM) top view image of our typical Ti circular Schottky contact is shown in figure 1(a), and the schematic three dimensional structure of the diode is displayed in figure 1(b). The current–voltage measurements were performed on Ti/*p*-type strained $Si_{0.95}Ge_{0.05}$ SBD over a temperature range of 100–300 K using a Keithley 2400 source Ammeter. A Janis closed cycle refrigeration system model 220c was used as the low-temperature cooling-device. For good thermal contact, the sample was mounted between two copper plates having a base directly fixed on the cold finger in the cryostat. A more detailed description of the used set-up can be found in reference [34].

For comparison, Pd/*n*-type strained $Si_{0.90}Ge_{0.10}$ SBD fabricated with the same area contacts was analyzed to confirm the validity of the reverse bias method. The *n*-type strained $Si_{0.96}Ge_{0.10}$ alloy with a thickness of about 480 nm and with phosphorous doping concentration of about 8×10^{16} cm^{-3}, was grown by RTCVD on a lightly doped (4-6$\times10^{16}$ cm^{-3}) Si buffer layer, which was grown on an n^+-Si

substrate. It should be noted that the forward electrical characteristics of Pd/*n*-type strained $Si_{0.90}Ge_{0.10}$ SBD have been previously performed and are reported elsewhere [35].

III. RESULTS AND DISCUSSION

The measured semi-log ln (*I*) vs. *V* plots in both forward and reverse directions of the Ti/*p*-strained $Si_{0.95}Ge_{0.05}$ SBD over the considered temperature range are shown in Fig. 2. The electrical characteristics of Ti/*p*-strained $Si_{0.95}Ge_{0.05}$ SBD were obtained by analyzing the I_R-V_R-T data at each measurement temperature under the assumption that the *TE* mode dominates the current transport in reverse bias. As can be seen, the Ti/*p*-$Si_{0.95}Ge_{0.05}$ SBD is always rectifying and obviously temperature dependent. As already reported elsewhere [20], these diodes are of high quality as demonstrated by their ideality factor close to unity. This implies that the current transport is driven by the *TE* mode. Hence, the variation of the current with temperature is simulated using the relationship within the *TE* model [36]:

$$I_{\mathrm{TE}} = I_{\mathrm{S}}\left[\exp\left(\frac{qV-R_sI}{nK_{\mathrm{B}}T}\right)-1\right] \quad (1)$$

with *n is* the ideality factor, R_s the series resistance, *V* the applied voltage and I_s the saturation current given by:

$$I_S = A^* S T^2 \exp(-\frac{\Phi_{Bp}}{k_B T}) \quad (2a)$$

where A^* is the effective Richardson constant, *S* the area of the diode, *T* the temperature of the junction, and Φ_{BP} the effective barrier height. A^* is calculated by using the linear dependence on the Ge content. The saturation current I_s is determined either by extrapolating the forward *I-V* characteristics to zero applied voltage or directly at reverse voltage V_R. Φ_{0Bp} stands for the zero bias barrier height when I_s is deduced from forward characteristic, Φ_{RBp} represents the reverse bias barrier height when I_s is deduced from reverse characteristic. In this case, the reverse saturation current I_s determined from the measurement of the current at an applied reverse voltage V_R is described by:

$$I_s \approx I_R(V_R) = A^* S T^2 \exp\left(-\frac{\Phi_{RBp}(V_R)}{k_B T}\right) \quad (2b)$$

It should be indicated that the effective barrier height $\Phi_{RBp}(V_R)$ depends on the reverse voltage bias and differs from the zero-field barrier Φ_{FBP} determined from C-V measurements under flat-band conditions. The zero-field barrier height Φ_{FBP} is related to zero bias and reverse bias barrier heights:

$$\Phi_{FBP} = \Phi_{Bp}^{I-V}(V) + \Delta\Phi_{im}(V) \quad (3)$$

where $\Delta\Phi_{im}(V)$ is the image force lowering given by [37]:

$$\Delta\Phi_{im}(V) = \left[\frac{qE_m(V)}{4\pi\varepsilon_{sc}}\right]^{\frac{1}{2}} \quad (4)$$

with E_m is the maximum electric field at the junction M/Sc, given by:

$$E_m(V_R) = \left[\frac{2qN_A(V_{bi}+|V_R|}{\varepsilon_{sc}}\right]^{\frac{1}{2}}. \quad (5)$$

N_A, V_{bi} and ε_{sc} (= $11.93\varepsilon_0$) being the p-type doping density, flat-band voltage, and permittivity of $Si_{0.95}Ge_{0.05}$ material, respectively.

As shown in Fig.2, the measured reverse current increases with increasing reverse bias in good agreement with *TE* model, where the SBH lowering due to image force effects was taken into account. In fact, the reverse bias dependence of the SBH deduced from the reverse characteristics was reported to exceed the expected lowering induced by image force effects [38]. In this scenario, the reverse current was considered to flow essentially through the patches exhibiting low SBHs localized at nonhomogeneous M/Sc contacts. The effective SBH $\Phi_{RBp}(V_R)$ is calculated for different applied reverse voltage bias at given temperature using equation (2b) and assuming $I_s = I_R$. The SBH deduced from the reverse bias I_R–V_R data as a function of temperature is displayed in Fig. 3. The temperature dependence of the zero-bias effective SBH Φ_{0Bp} deduced from I_F–V_F measurements is also displayed in this figure for comparison. It can be clearly observed that the barrier heights deduced from both the forward and reverse bias increase with the temperature. The value of SBH from reverse bias is however lower than the forward bias counterpart, regardless the temperature. Actually, the difference

in the SBH values obtained from either the reverse or forward bias *I–V* characteristics is explained in terms of the image force lowering (see Table I). The increase of the barrier height as deduced from I_F-V_F characteristics upon temperature has been attributed to the presence of *BH*i at M/Sc contacts [6, 12-21]. A similar behavior in the reverse bias mode is observed as shown in Fig. 3. Like the forward mode, the Werner-Güttler model [16] has been used to determine the reverse bias mean value ($\overline{\Phi}_{RBp}$) and its standard deviation (σ_{Rs}):

$$\Phi_{RBp}(\mathrm{V_R}) = \overline{\Phi}_{RBp}(\mathrm{V_R}) - \frac{q^2\sigma_{Rs}^2(\mathrm{V_R})}{2k_BT} \qquad (6)$$

As shown in Fig. 4, the SBH measured at different reverse bias fits linearly with the inverse of temperature, in good agreement with equation (6). This is a direct consequence of the presence of lateral *BH*i at Ti/*p*- strained $Si_{0.95}Ge_{0.05}$ interface. From the straight lines of the plots displayed in Fig. 4, the reverse bias mean barrier height $\overline{\Phi}_{RBp}$ and its standard deviation σ_{Rs} is deduced from the intercept at the ordinate and the slope, respectively. The corresponding values for different applied bias voltage are plotted in Fig. 5 and summarized in Table I. One can notice a decrease of $\overline{\Phi}_{RBp}$ and an increase of σ_{Rs} when the applied reverse bias increases. The decrease of $\overline{\Phi}_{RBp}$ with increasing reverse bias is consistent with the respective increase of Schottky barrier lowering due to the image force effects. The image force lowering is calculated according to equation 4 as a function of the reverse bias, by taking into account the doping density in the *p*-strained $Si_{0.95}Ge_{0.05}$ epilayer. The calculated image force lowering $\Delta\Phi_{im}(\mathrm{V_R})$ values at different reverse bias V_R are also listed in Table I. After including the image force lowering effect correction, the obtained SBH ($\overline{\Phi}_{RBp} + \Delta\Phi_{im}(V_R)$) is equivalent to the Schottky barrier height determined under flat band conditions. The corrected SBH is found to be independent of the applied reverse bias. Therefore, the measured reverse mean barrier height values are modified solely by the image force effects. This confirms that the *TE* mode dominates the conduction transport mechanism in the reverse current-voltage characteristics. Moreover, a correlation between the increases of σ_{Rs} with reverse bias is well observed. This indicates that the inhomogeneities of SBH can be interpreted in terms of the variation of the barrier height

distribution with applied reverse bias. Indeed, the standard deviation decreases with decreasing electric field at M/Sc interface. In fact, σ_{Rs} decreases to zero on approaching the flat band conditions at zero-electric field.

The inhomogeneities induced barrier height fluctuations is then shown to affect considerably the temperature dependence of the reverse I_R–V_R characteristics. This can be pointed out in the conventional Richardson plots, namely ln (I_s/T^2) vs. $1/k_BT$ (equation 7).

$$\ln\left(\frac{I_R}{T^2}\right) = \ln\left(A^* S\right) - \left(\frac{\Phi_{RBp}}{k_B T}\right) \tag{7}$$

The ln (I_R/T^2) vs. $1/k_BT$ plot is expected to show a linear behavior with a slope given by a reverse bias SBH at 0 K, $\Phi_{RBp}(T=0)$ and an intercept at the ordinate given by an experimental Richardson constant, A^*. From the experimental data reported in Fig.2, the value of the reverse saturation current at a given applied reverse bias I_s (V_R) is determined for each temperature. The corresponding Richardson ln (I_R/T^2) vs. $1/k_BT$ plot for Ti/*p*-strained $Si_{0.95}Ge_{0.05}$ SBD is shown in figure 6. As can be seen, the fit of the experimental data exhibit nonlinear dependence at low temperatures (ln (I_R/T^2) axis). The values of the activation energy ($E_a = \Phi_{RBp}(T=0)$) and Richardson constant A^* were deduced from the slope and the intercept at the ordinate of the linear region of these plots, respectively [39]. The results are given in Table. I. The extracted experimental values of the Richardson's constant from the conventional plots are more than two-order of magnitude lower than the theoretical value for *p*-type strained $Si_{0.95}Ge_{0.05}$ (32 A cm^{-2} K^{-2}) [40]. The extracted SBHs are almost two-times lower than the reverse bias mean SBHs values extracted from the plot of $\Phi_{RBp}(V_R)$ vs. $1/2k_BT$ (see figure 4) at different reverse voltages. The low extracted values of A^* and $\Phi_{RBp}(T=0)$ as well as the distortion in the conventional Richardson plots at lower temperature are mainly attributed to the SBH fluctuations due to inhomogeneities at the Ti/*p*-strained $Si_{0.95}Ge_{0.05}$ interface.

Several reasons have been considered to explain for the presence of *BH*i at M/Sc contacts. Besides interface states and/or defects that are usually at the origin of this *BH*i, the alloy fluctuations

in compound semiconductors may also be at the origin of *BH*i. It has been previously reported that *BH*i at Au/AlInGaN Schottky contacts with different indium and aluminum content is mainly due to alloy fluctuation [14]. In our case, the Ge atoms are randomly distributed within the $Si_{1-x}Ge_x$ alloy and thus their distribution in the $Si_{0.95}Ge_{0.05}$ is assumed to be purely statistical. Such random distribution of Ge atoms leads to a fluctuation in the band gap energy (E_g). Since the major part of the band gap variation ΔE_g at the $Si_{1-x}Ge_x$/Si heterojunction is contained in the valence band ($\Delta E_g\,(x) = \Delta E_V\,(x)$) [41-44], the fluctuation in the band gap of $Si_{1-x}Ge_x$ will induce a fluctuation in the valence band. Subsequently a fluctuation of the barrier height on *p*-type $Si_{1-x}Ge_x$ is expected. A schematic energy band diagram between metal and *p*-type $Si_{1-x}Ge_x$ showing fluctuation in the valence band is illustrated in Fig. 7.

In order to take account of the spatially inhomogeneous SBH, a modified Richardson plot is obtained by combining equations (2b) and (7) giving rise to equation (8):

$$\ln\left(\frac{I_R}{T^2}\right) - \left(\frac{q^2\sigma_{RS}^2}{2k_B^2T^2}\right) = \ln\left(A^*S\right) - \frac{\overline{\Phi}_{RBp}}{k_BT} \tag{8}$$

The new plot $\ln\left(\frac{I_R}{T^2}\right) - \left(\frac{q^2\sigma_{RS}^2}{2k_B^2T^2}\right)$ vs. $1/k_BT$ yields a straight line whose its slope is associated with the reverse bias mean SBH and its y-axis intercept as the new Richardson constant A^* (see Fig 6). The new Arrhenius plots are linear over the whole temperature range for the investigated reverse voltages. The extracted Richardson constant shows a small bias dependence, increasing between –1.0 V and -2.5 V and followed by a slight decrease beyond (see Table 1). The mean value of Richardson constant extracted for different reverse bias (38.4 A cm^{-2} K^{-2}) is in fair agreement with the predicted theoretical value. On the other hand, the slope of the curves that represents the reverse bias mean SBH $\overline{\Phi}_{RBp}$ were calculated at each reverse bias and the values match exactly, within the calculated experimental error, with those extracted from the plots Φ_{RBp} versus $1/T$ reported in figure 4 (Table I). We therefore conclude from this analysis that the temperature dependence of the reverse *I-V-T*

characteristics of Ti/*p*-strained $Si_{0.95}Ge_{0.05}$ contacts can be successfully explained based on *TE* model that accounts for the inhomogeneities of Schottky barrier height.

It is worth to mention that the reverse bias method has been applied to investigate *BH*i in another structure, namely Pd/*n*-type $Si_{0.90}Ge_{0.10}$. The corresponding data of the reverse current versus voltage measured at temperatures between 100 and 300 K are shown in Fig. 8. The results are well interpreted on the basis of *TE* model associated with Gaussian distribution of barrier heights. The first observation that arises from the initial analysis of the measured reverse *I-V* between the two samples concerns the leakage current. As compared to Ti//*p*-strained $Si_{0.95}Ge_{0.05}$, the Pd/*n*- type $Si_{0.90}Ge_{0.10}$ SBD reveals an enhanced leakage current in the low temperature range (100-140 K) and at high reverse bias (3V). This may indicate that at temperature below 140 K, the presence of other current transport mechanisms such as recombination-generation current can be expected. This later mode is usually more pronounced in the reverse bias as compared to the forward bias counterpart. On the other side, the *TE* current mode might dominate the current transport in the temperature range 140-300 K. Similarly, using the same procedure as in the case of Ti/*p*-strained $Si_{0.95}Ge_{0.05}$, and following the SBH distribution model proposed by Werner and Güttler, the barrier height deduced from reverse bias for Pd/*n*- $Si_{0.90}Ge_{0.10}$ is found to be temperature dependent (see Fig. 8b). In fact, the behavior in the reverse bias is found to be similar to that in the forward bias. To further examine the *BH*i at Pd/*n*-type strained $Si_{0.90}Ge_{0.10}$, the plot of $\Phi_{RBn}(V_R)$ vs. $1/2k_BT$ should give a straight linear according to equation (6). Such a plot is shown in Fig. 8c and the results of the data fitting leads to the mean reverse bias $\overline{\Phi}_{RBn}$ and its standard deviation σ_{Rs} as summarized in Table II. When taking into account of the image force lowering, usually more important in the reverse bias regime, the corrected SBH$\overline{\Phi}_{RBn} + \Delta\Phi_{im}(V_R)$) is also found independent of the applied reverse bias within the calculated experimental error. Based on the *BH*i model, a plot of the modified $\ln(\frac{I_R}{T^2}) - (\frac{q^2\sigma_{RS}^2}{2k_B^2T^2})$ vs. $1/k_BT$, according to equation (8) yields a straight line with the slope giving the reverse bias mean SBH $\overline{\Phi}_{RBn}$ and the intercept giving the modified Richardson constant *A**as shown in Fig. 8c. Actually, the plots of

experimental data shown in Fig. 8d were all well fitted using rather two straight lines instead of a single straight line with a transition occurring at 140 K. Here again the values of A^* obtained from these plots are in good agreement with the theoretical value of 112 $A.K^{-2}.cm^{-2}$ obtained for *n*-type $Si_{0.90}Ge_{0.15}$ [36, 37]. The temperature dependent reverse current-voltage characteristics of Pd/*n*-strained type $Si_{0.90}Ge_{0.10}$ structure is successfully explained on the basis of *TE* mechanism with a Gaussian distribution of the barrier height. It is worth noting that the reverse mean values of barrier height, deduced from Fig. 8d matches exactly with those obtained from the Φ_{RBn} vs. $1/2k_BT$ reported in Fig 8c. We conclude that the *BH*i at Pd/*n*-type $Si_{0.90}Ge_{0.10}$ using reverse electrical characteristics can be satisfactorily explained by inhomogeneous model with Gaussian distribution of SBH.

IV. Conclusion

In this work, we have demonstrated that the temperature dependent reverse current-voltage characteristics can be used to investigate the barrier height inhomogeneities at Ti/*p*-type strained $Si_{1-x}Ge_x$Schottky contacts. The transport mode in the reverse bias is governed by the *TE* mode associated with a Gaussian SBH distribution. The abnormally temperature dependent of SBH deduced from reverse current-voltage characteristics is found to be similar to that using forward current-voltage characteristics. The decrease of homogeneous SBH $\overline{\Phi}_{RBp}$ and the increase of standard deviation σ_{Rs} with increasing applied reverse bias are shown to be related to the increase of Schottky barrier lowering due to the image force effects and the high degree of inhomogeneity at Ti/*p*-strained $Si_{0.95}Ge_{0.05}$ interface, respectively. The reverse bias values for Richardson constant A^*, extracted from the modified plots based on *BH*i model, are close to the theoretical value of 32 A cm^{-2} K^{-2} for *p*-type $Si_{0.95}Ge_{0.05}$. Consistent results for the four applied reverse voltages are well described by the model of potential fluctuations. Moreover, the utilization of the reverse bias method is corroborated by the results obtained on Pd/*n*-type $Si_{0.90}Ge_{0.10}$ SBD shown in this work.

References

[1] S. S. Cohen and G. S. Gildenblat, Metal-Semiconductor Contacts and Devices, VLSI Electronics edited by N. G. Einspruch (Acadenic Press, New York (1986), Vol. **13**.

[2] E. Sano, IEEE Trans. Electron. Dev. **37**, 1964 (1990).

[3] A. Ketterson, M. Tong, J. W. Seo, K. Nummila, K. Y. Cheng, J. Morikuni, S. Kang and I. Adesida, J. Vac. Sci. Technol. B **10**, 2936 (1992).

[4] W. Zhao, Y. Zhao and M. Miao, Microelectronics Journal. **136**, 105775 (2023).

[5] R.T. Tung, Appl. Phys. Rev**. 1**, 011304 (2014).

[6] F. Iucolano, F. Roccaforte, F. Giannazzo and V. Raineri, J. Appl. Phys. **104**, 093706 (2008).

[7] K. Bouziane, M. Mamor and F. Meyer, Appl. Phys. A **81**, 209 (2005).

[8] H. Özerli, A. Bekereci, A. Türüt and Ş. Karataş, Journal of Alloys and Compounds. **718**, 5 (2017).

[9] M. Cavas, F. Yakuphanoglu and Ş. Karataş, Indian Journal of Physics. **91**, 413 (2017).

[10] H. Seymen, N. Berk, I. Orak, and Ş. Karataş, J Mater Sci: Mater Electron**. 33**, 19656 (2022).

[11] Ş. Karataş and M. Çakar, Synthetic Metals **159**, 347 (2009).

[12] N. Yıldırım, K. Ejderha and A. Turut, J. Appl. Phys. **108**, 114506 (2010).

[13] A. Tataroğlu and F.Z. Pür. Phys. Scr. **88**, 015801 (2013).

[14] M. A. Laurent, G. Gupta, D. J. Suntrup, S. P. DenBaars and U. K. Mishra, J. Appl. Phys. **119**, 064501 (2016).

[15] Y. Atasoy, M. A. Olgar and E. Bacaksiz, J. Mater Sci: Mater Electron. **30**, 10435 (2019).

[16] J. H. Werner and H. H. Güttler, J. Appl. Phys. **69**, 1522 (1991).

[17] M. Mamor, K. Bouziane, A. Tirbitine and H. Alhamrashdi, Superlattices and Microstructures. **72**, 344 (2014).

[18] A. B. Uluşan¸ A. Tataroğlu, Y. A. Kalandaragh and Ş¸ Altındal, J. Mater. Sci.: Mater. Electron. **29**,159 (2018).

[19] Ş. Atindal, A. F. Özdemir, Ş. Aydoğan and A. Türüt. J Mater Sci: Mater Electron**. 33**, 12210 (2022).

[20] M. Mamor, K. Bouziane and A. Tirbiyine, J. Mater. Sci: Mater Electron. **25**, 1527 (2014).

[21] A. Venter, D. M. Murape, J. R. Botha, F. D. Auret, Thin Solid Films. **574**, 32 (2015).

[22] H. Palm, M. Arbes and M. Schulz, Phys. Rev. Lett. **71**, 2224 (1993).

[23] R. Buzio, A. Gerbi, D. Marrè, M. Barra and A. Cassinese, Organic Electronics. **18**, 44 (2015).

[24] C. A. Durcan, R. Balsano and V. P. LaBella, J. Appl. Phys. **117**, 245306 (2015).

[25] S. Zhu, R. L. Van Meirhaeghe, C. Detavernier, G. P. Ru, B. Z. Li and F. Cardon, Solid State Communication. **112**, 611 (1999).

[26] R. Buzio, A. Gerbi, E. Bellingeri and D. Marré, Appl. Phys. Lett. **113**, 141604 (2018).

[27] S. K. Tripathi and M. Sharma, J. Appl. Phys. 111, 074513 (2012)

[28] H. C. Lin, P. D. Ye and G. D. Wilk, Appl. Phys. Lett. **87**, 182904 (2005).

[29] S. Alialy, D. E. Yıldız and Ş. Altındal, J. Nanoelectronics and Optoelectronics. **11**, 626 (2016).

[30] K. Sreenu, C. V. Prasad and V. R. Reddy, J. Electron. Mater. **46**, 5746 (2017).

[31] Ç. Ş. Güçlü, A. F. Özdemir, D. A. Aldemir and Ş. Altındal, J. Mater Sci: Mater Electron. **32**, 5624 (2021).

[32] I. Orak, A. Kocyiğit, and Ş. Karataş, Silicon. **10**, 2109 (2018).

[33] H. B. Michaelson, J. Appl. Phys. **48**, 4729 (1977).

[34] A. Sellai and P. Dawson, J. Cryst. Growth. **288**, 166 (2006).

[35] M. Mamor, A. Sellai, K. Bouziane, S. H. Al Harthi, M. Al. Busaidi and F. S. Gard, J. Phys. D: Appl. Phys. **40**, 1351 (2007).

[36] E. H. Rhoderick, and R. H. Williams, *Metal–Semiconductor contacts*, 2nd ed. (Clarendon, Oxford, 1988), p 40.

[37] M. Sze, *Physics of Semiconductor Devices, 2*nded. (Wiley, New York, 1981), p 256.

[38] J. P. Sullivan, R. T. Tung, M. R. Pinto and W. R. Graham, J. Appl. Phys. **70**, 7403 (1991).

[39] F. M. Coşkun, O. Polat, M. Coşkun, A. Turut, M. Caglar, Z. Durmus, and H. Efeoğlu, J. Appl. Phys. **125**, 214104 (2019).

[40] G. P. Ru, G. W. Wang, Y. L. Jiang, W. Huang, X. P. Qu, S. Y. Zhu and B. Z. Li, J. Vac. Sci. Technol. B **21**, 1301 (2003).

[41] C. G. Van de Walle and R. M. Martin, Phys. Rev. B **34**, 5621 (1986).

[42] V. Aubry, F. Meyer, P. Warren and D. Dutartre, Appl. Phys. Lett. **63**, 2520 (1993).

[43] R. L. Jiang, J. L. Liu, J. Li, Y. Shi and Y. D. Zheng, Appl. Phys. Lett. **68**, 1123 (1996).

[44] M. Mamor, O. Nur, M. Karlsteen, M. Willander and F.D. Auret, J. Appl. Phys. **86**, 6890 (1999).

"Statements and Declarations"

The authors declare that no funds, grants, or other support were received during the preparation of this manuscript.

"Competing Interests"

The authors have no relevant financial or non-financial interests to disclose.

"Author Contributions"

All authors contributed to the study conception and design. Material preparation, data collection and analysis were performed by Mohammed Mamor, Khalid Bouziane, Hind Chakir and Pierre Ruterana. All authors read and approved the final manuscript.

" Data Availability Statement"

The datasets generated during and/or analyzed during the current study are available from the corresponding author on reasonable request.

TABLE I. Experimental data for Ti/*p*-strained $Si_{0.95}Ge_{0.05}$/Si SBD extracted from both reverse bias I_R–V_R and forward bias I_F–V_F curves.

Bias (V)	$\overline{\Phi}_{RBp}$ (V_R) *Reverse I-V (eV)*	$\Delta\Phi_{im}$ *(meV)*	$\Phi_{FBp} = \overline{\Phi}_{RBp} + \Delta\Phi_{im}$	σ_{Rs} (mV)	A^* [(b)] A.cm^{-2}.K^{-2}	A^*[(c)] A.cm^{-2}.K^{-2}	$\overline{\Phi}_{RBp}$[(c)] *(eV)*
0	0.546±0.005[(a)]	37 [(a)]	0.583 ±0.005[(a)]	67.00[(a)]	0.06[(a)]	35.5[(a)]	0.550±0.005[(a)]
-1	0.541±0.005	50	0.591±0.005	74.43	0.04	35.1	0.538±0.005
-2	0.536±0.005	57	0.593 ±0.005	77.72	0.06	36.2	0.536±0.005
-2.5	0.530±0.005	60	0.590 ±0.005	78.10	0.06	43.4	0.535±0.005
-3	0.524±0.005	62	0.586 ±0.005	78.29	0.04	41.7	0.528±0.005

[(a)] Electrical parameters as determined only from forward I_F-V_F characteristics.

[(b)] Richardson constant A^*as determined from conventional plot ln (I_R/T^2) vs. ($1/k_BT$).

[(c)] Richardson constant $A^*$and $\overline{\Phi}_{RBp}$ as determined from modified plot $\ln\left(\frac{I_R}{T^2}\right) - \left(\frac{q^2\sigma_{RS}^2}{2k_B^2T^2}\right)$ vs. ($1/k_BT$).

TABLE II. Experimental data for Pd/*n*-strained $Si_{0.90}Ge_{0.10}$/Si SBD extracted from both reverse bias I_R–V_R and forward bias I_F–V_F curves.

Bias (V)	$\overline{\Phi}_{RBp}$ (V_R) *Reverse I-V (eV)*	$\Delta\Phi_{im}$ *(meV)*	$\Phi_{FBp} = \overline{\Phi}_{RBp} + \Delta\Phi_{im}$	σ_{Rs} (mV)	A^*[(b)] A.cm^{-2}.K^{-2}	$\overline{\Phi}_{RBp}$[(b)] *(eV)*
0	0.805±0.005[(a)]	39 [(a)]	0.84 ±0.005[(a)]	84 [(a)]	110[(a)]	0.806±0.005[(a)]
-1	0.796±0.005	50	0.8451±0.005	111	109	0.787±0.005
-2	0.766±0.005	57	0.823 ±0.005	111	100	0.758±0.005
-2.5	0.762±0.005	60	0.822 ±0.005	112	91	0.751±0.005
-3	0.761±0.005	62	0.823 ±0.005	115	127	0.744±0.005

[(a)] Electrical parameters as determined only from forward I_F-V_F characteristics.

[(b)] Richardson constant $A^*$and $\overline{\Phi}_{RBp}$ as determined from modified plot $\ln\left(\frac{I_R}{T^2}\right) - \left(\frac{q^2\sigma_{RS}^2}{2k_B^2T^2}\right)$ vs. ($1/k_BT$).

FIGURE CAPTIONS

Fi.g.1. (a) A SEM image of Ti circular Schottky contacts. (b) A Schematic cross section view of the Schottky barrier diode.

Fig. 2. (Color online) Experimental reverse and forward *I–V* curves of Ti/*p*-strained $Si_{0.95}Ge_{0.05}$ SBD at different temperatures.

Fig. 3. (Color online) Variation of the effective reverse barrier heights Φ_{RBp} as a function of temperature of Ti/*p*-strained $Si_{0.95}Ge_{0.05}$ SBD for different applied reverse bias. For comparison, the temperature dependence of the effective zero-bias SBH Φ_{0Bp}as deduced from I_F-V_F characteristics is also shown.

Fig. 4. (Color online) The effective reverse barrier heights Φ_{RBp}vs. $1/2k_BT$ curves of Ti/*p*-strained $Si_{0.95}Ge_{0.05}$ SBD according to inhomogeneous model [12].

Fig. 5. Variation of the reverse-bias means barrier height $\bar{\Phi}_{RBp}$ and the reverse-bias standard deviation σ_{Rs} as a function of the applied reverse bias.

Fig. 6. (Color online) Conventional Richardson plots ln (I_R/T^2) vs. ($1/k_BT$) and modified Richardson plots $\ln(\frac{I_R}{T^2})-(\frac{q^2\sigma_{RS}^2}{2k_B^2T^2})$ vs. ($1/k_BT$) drawn for different applied reverse bias.

Fig. 7. A schematic energy band diagram of Ti/*p*-type $Si_{1-x}Ge_x$ Schottky contacts (not to scale).

Fig. 8. (Color online) Experimental reverse and forward *I–V* curves of Pd/*n*-strained $Si_{0.90}Ge_{0.10}$ SBD at different temperatures (Fig. 8 a). Fig. 8b, Fig 8c and Fig .8d are the variation of the effective reverse barrier heights Φ_{RBp}as a function of temperature, the effective reverse barrier heights Φ_{RBp}vs. $q/2k_BT$ curves and the modified Richardson plots $\ln(\frac{I_R}{T^2})-(\frac{q^2\sigma_{RS}^2}{2k_B^2T^2})$ vs. ($1/k_BT$) drawn for different applied reverse bias, respectively.

Fig. 1

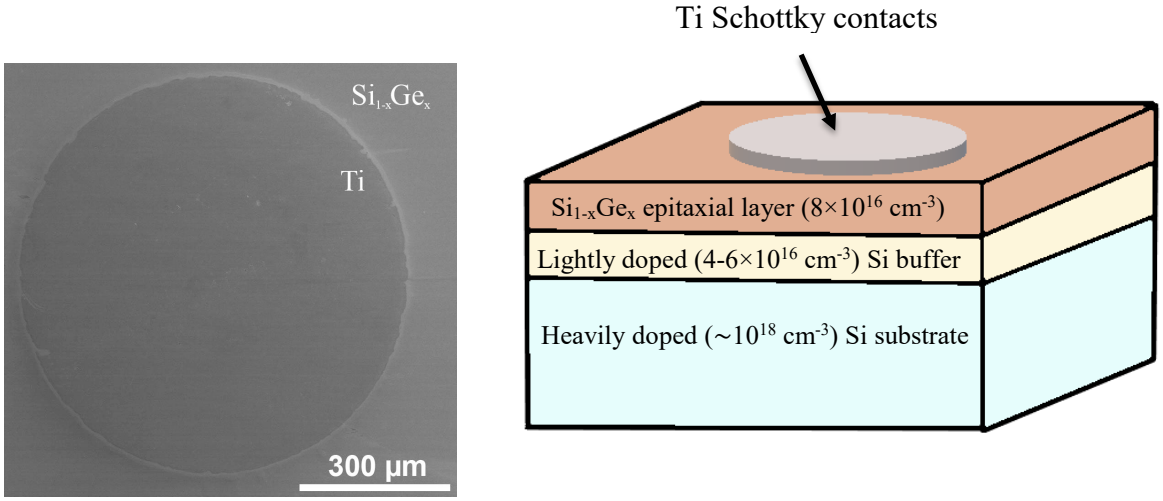
Si1-xGex
Ti
300 μm
Ti Schottky contacts
Si1-xGex epitaxial layer (8×10^16 cm^-3)
Lightly doped (4-6×10^16 cm^-3) Si buffer
Heavily doped (~10^18 cm^-3) Si substrate

(a) **(b)**

Fig. 2

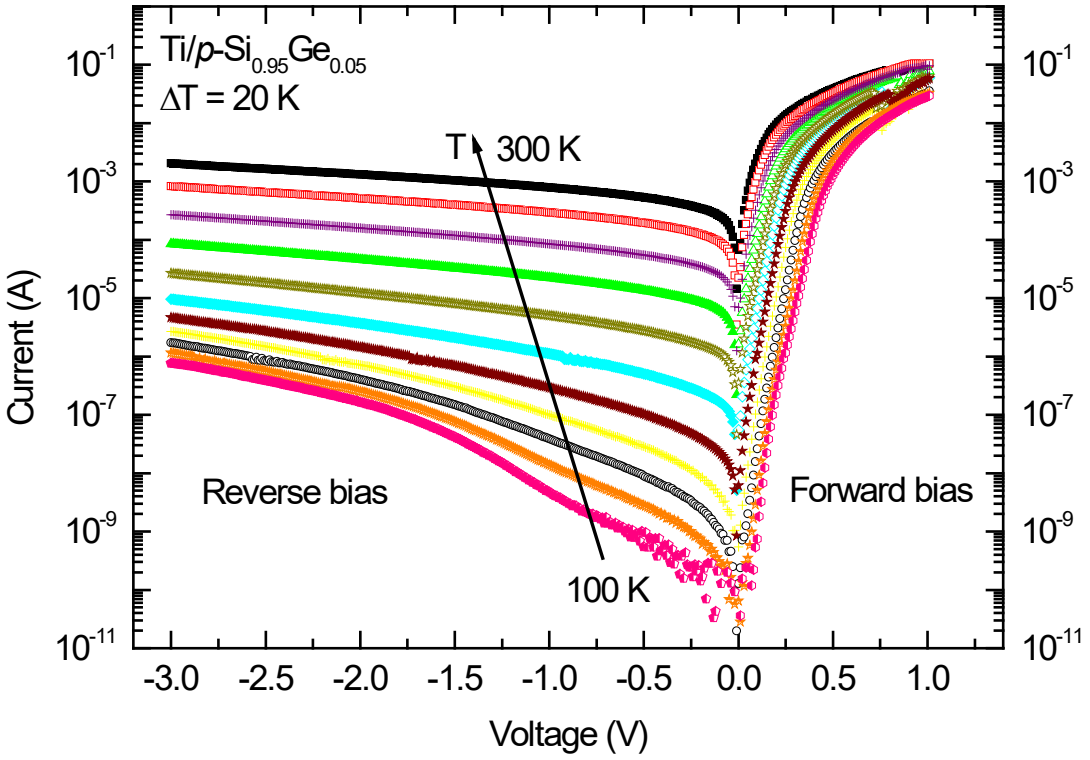
Ti/p-Si0.95Ge0.05
ΔT = 20 K
T
300 K
100 K
Reverse bias
Forward bias
Current (A)
Voltage (V)
10-1
10-3
10-5
10-7
10-9
10-11
-3.0
-2.5
-2.0
-1.5
-1.0
-0.5
0.0
0.5
1.0

Fig. 3

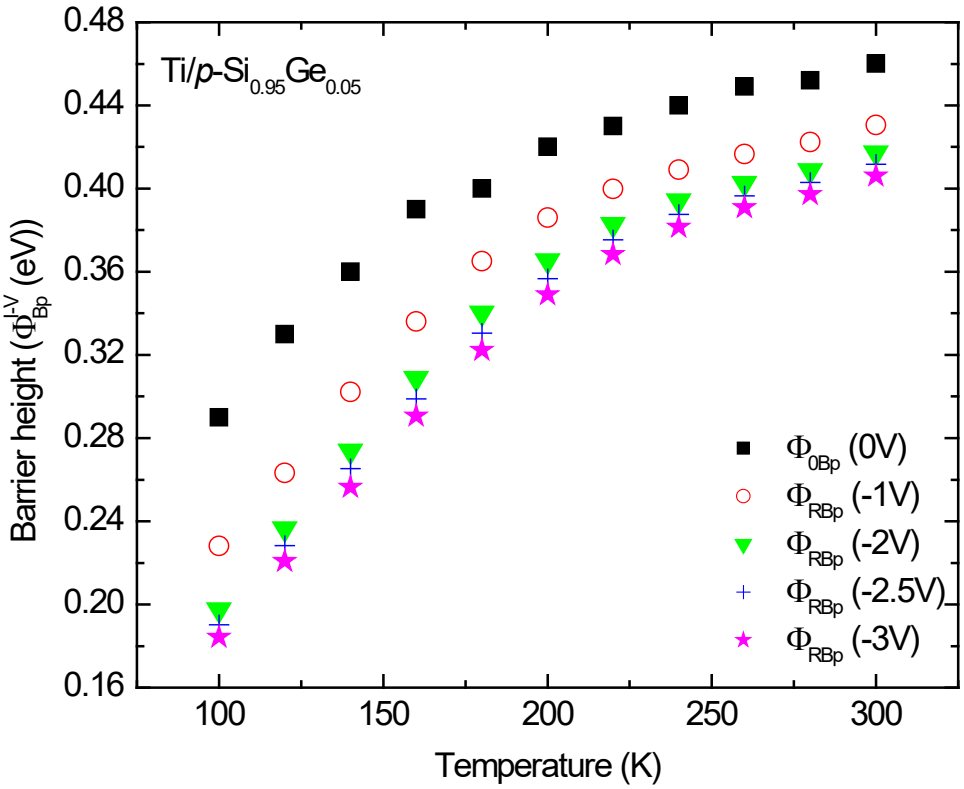
Ti/p-Si0.95Ge0.05
Barrier height (Φ_Bp^I-V (eV))
Temperature (K)
0.48
0.44
0.40
0.36
0.32
0.28
0.24
0.20
0.16
100
150
200
250
300
Φ0Bp (0V)
ΦRBp (-1V)
ΦRBp (-2V)
ΦRBp (-2.5V)
ΦRBp (-3V)

Fig. 4

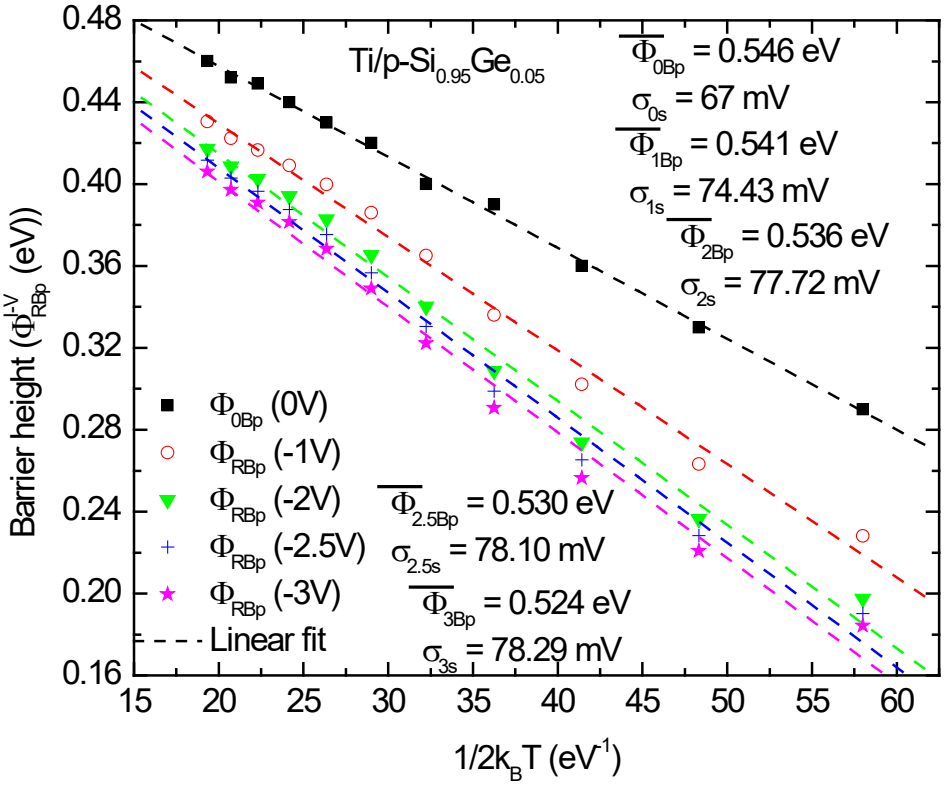
Ti/p-Si0.95Ge0.05
$\overline{\Phi}_{0Bp}$ = 0.546 eV
σ_{0s} = 67 mV
$\overline{\Phi}_{1Bp}$ = 0.541 eV
σ_{1s} = 74.43 mV
$\overline{\Phi}_{2Bp}$ = 0.536 eV
σ_{2s} = 77.72 mV
$\overline{\Phi}_{2.5Bp}$ = 0.530 eV
$\sigma_{2.5s}$ = 78.10 mV
$\overline{\Phi}_{3Bp}$ = 0.524 eV
σ_{3s} = 78.29 mV
Φ_{0Bp} (0V)
Φ_{RBp} (-1V)
Φ_{RBp} (-2V)
Φ_{RBp} (-2.5V)
Φ_{RBp} (-3V)
Linear fit
Barrier height (Φ_{RBp}^{I-V} (eV))
1/2k$_B$T (eV^{-1})
0.48
0.44
0.40
0.36
0.32
0.28
0.24
0.20
0.16
15
20
25
30
35
40
45
50
55
60

Fig. 5

Bp

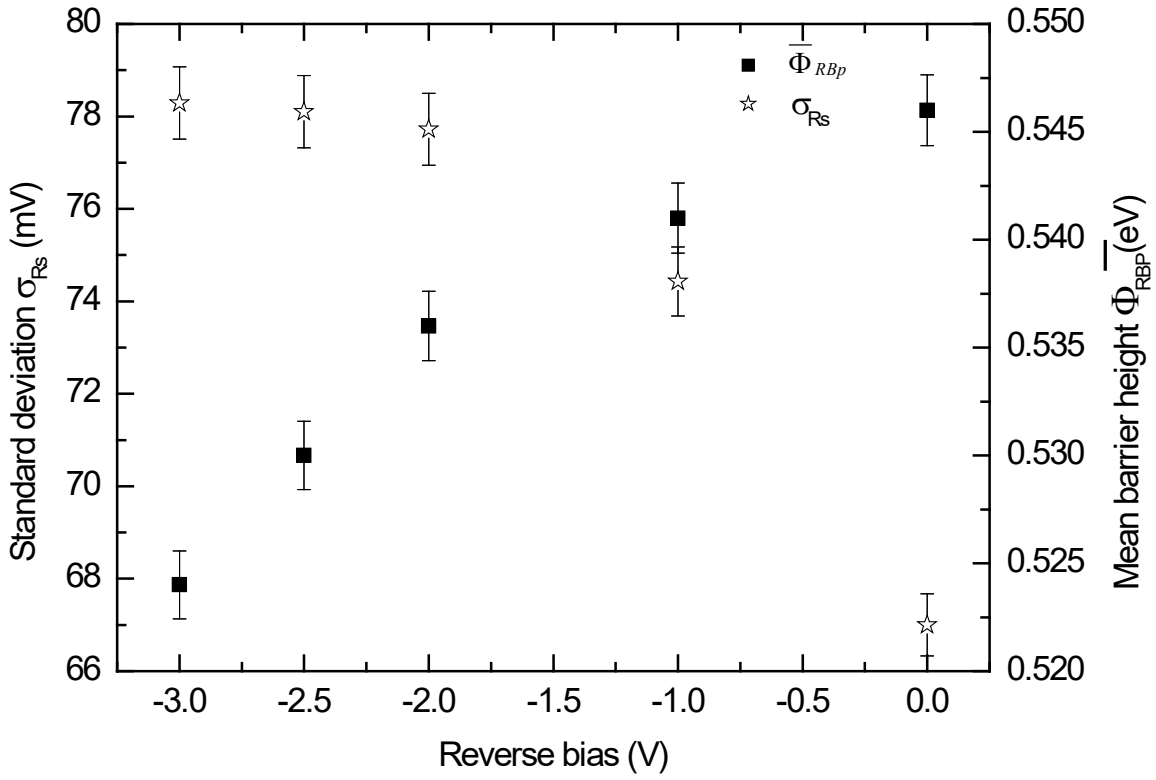
80
78
76
74
72
70
68
66
0.550
0.545
0.540
0.535
0.530
0.525
0.520
-3.0
-2.5
-2.0
-1.5
-1.0
-0.5
0.0
Reverse bias (V)
Standard deviation σRs (mV)
Mean barrier height ΦRBP (eV)
Φ RBp
σRs

Fig. 6

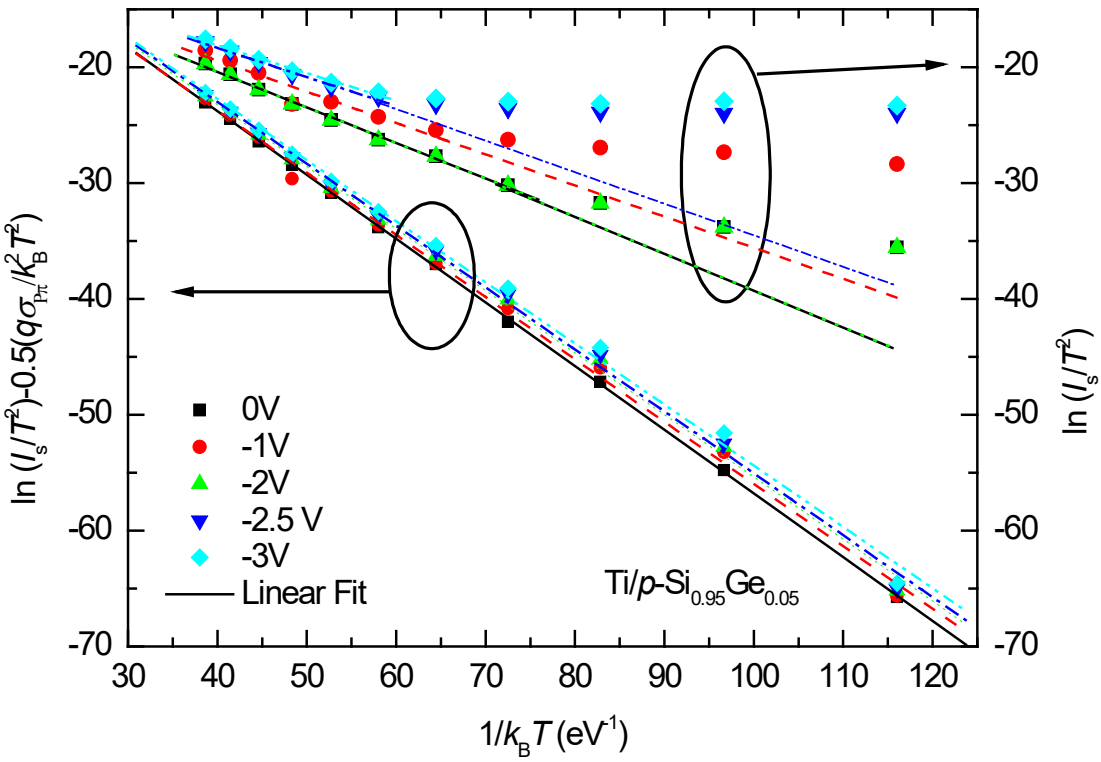
-20
-30
-40
-50
-60
-70
30
40
50
60
70
80
90
100
110
120
$\ln(I_s/T^2)-0.5(q\sigma_{p\pi}/k_B^2T^2)$
$\ln(I_s/T^2)$
$1/k_BT\ (eV^{-1})$
0V
-1V
-2V
-2.5 V
-3V
Linear Fit
Ti/*p*-$Si_{0.95}Ge_{0.05}$

Fig. 7

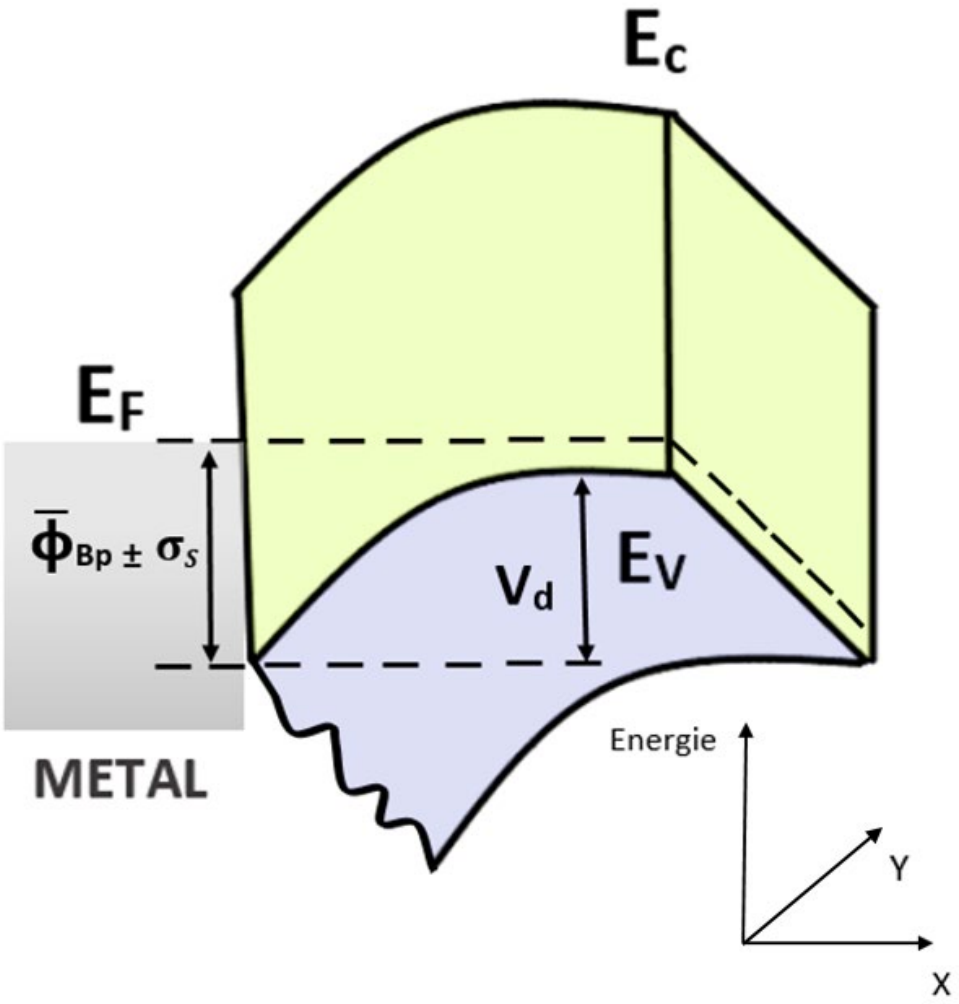

Fig. 8

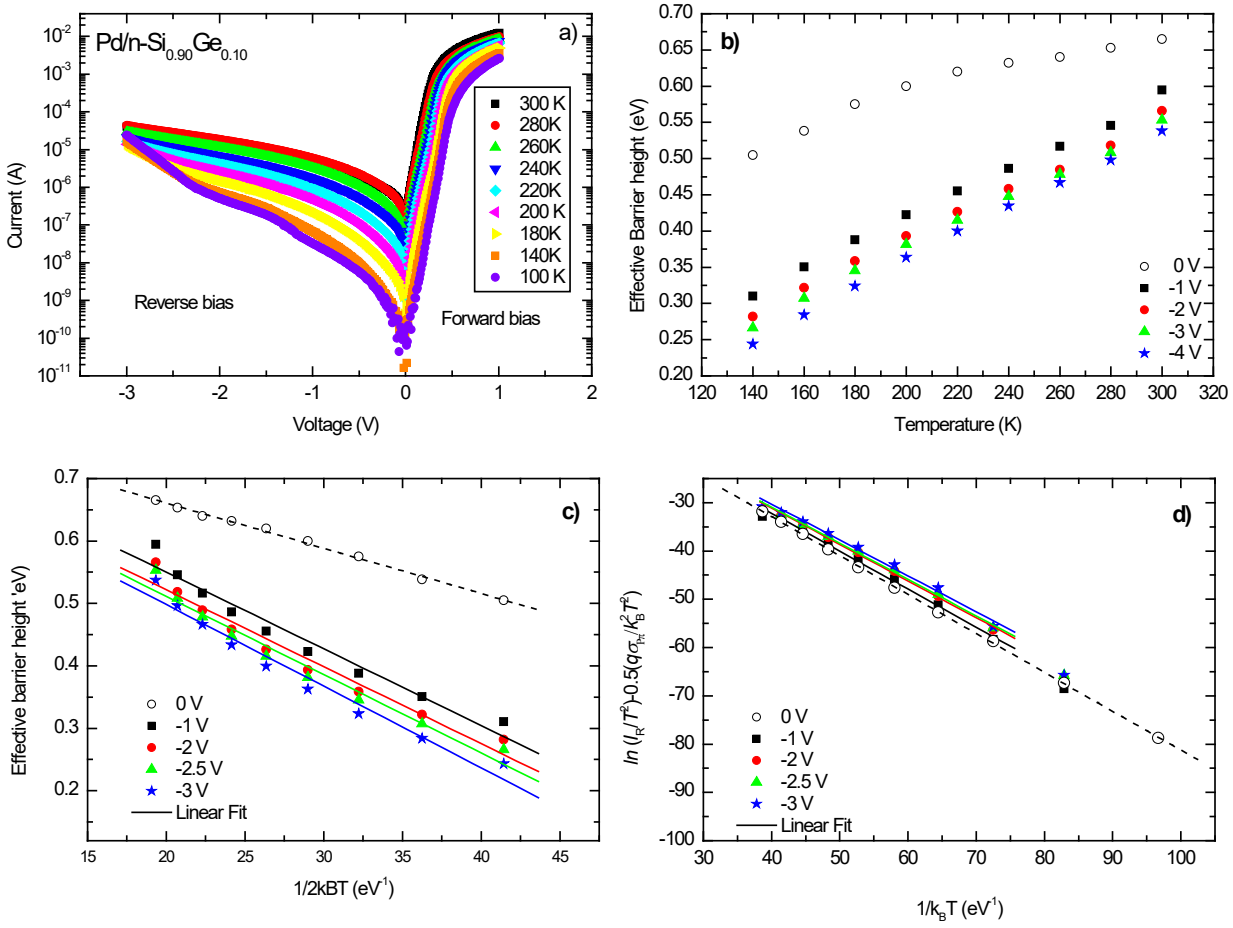
a)
Pd/n-Si0.90Ge0.10
Current (A)
Voltage (V)
300 K
280K
260K
240K
220K
200 K
180K
140K
100 K
Reverse bias
Forward bias
b)
Effective Barrier height (eV)
Temperature (K)
0 V
-1 V
-2 V
-3 V
-4 V
c)
Effective barrier height 'eV)
1/2kBT (eV-1)
0 V
-1 V
-2 V
-2.5 V
-3 V
Linear Fit
d)
ln (IR/T2)-0.5(qσb2/kB2T2)
1/kBT (eV-1)
0 V
-1 V
-2 V
-2.5 V
-3 V
Linear Fit